Passive 2.45 GHz TDMA based Multi-Sensor Wireless Temperature Monitoring System: Results and Design Considerations

doi: 10.1109/ULTSYM.2006.366

Passive 2.45 GHz TDMA based Multi-Sensor Wireless Temperature Monitoring System: Results and Design Considerations

J. H. Kuypers*, S. Tanaka, M. Esashi
Department of Nanomechanics
Tohoku University
Sendai, Japan
*jan@mems.mech.tohoku.ac.jp

D. A. Eisele, L. M. Reindl
Laboratory for Electrical Instrumentation
IMTEK, University of Freiburg
Freiburg, Germany

***Abstract*—This paper presents a TDMA (time division multiple access) based wireless temperature monitoring system using 2.45 GHz passive surface acoustic wave (SAW) delay line sensors. A three-step resolution refinement scheme using a combined delay and phase evaluation is proposed. Using a transmission power of 2 dBm (1.59 mW) a temperature accuracy of 0.19 K and 0.1 K (6σ), were achieved for an interrogation distance of 1.4 m, and 1.3 m, respectively. The sensor design is discussed using experimental results concerning the relationship between the SNR (signal to noise ratio) of the sensors and the accuracy in time delay or phase measurement. Also, the direct electron beam writing on chemically-reduced (black) $LiNbO_3$ is described.**

Keywords-Wireless SAW sensors, delay line sensors, TDMA, K-Model, SNR (signal to noise ratio)

I. INTRODUCTION

Wireless sensor technology possesses a large potential concerning measurement flexibility, monitoring of moving objects, and measurement in hazardous environments. This is a key technology for an emerging ubiquitous computing society, in which tiny wireless sensors will be embedded in virtually all items around us. The application of surface acoustic wave (SAW) based sensors [1][2] has the advantage of being passive and thus free from the replacement of batteries, featuring a long lifetime and high reliability. In addition, the wireless interrogation of these passive sensors with read-out ranges of up to 5 m is possible, which is considerably larger than inductively powered sensors using 13.56 MHz.

In previous studies [1][3], SAW based sensors were applied to wireless temperature measurement, and the possibility of time division multiple access (TDMA) scheme was suggested. However, the TDMA of SAW based sensors has not been demonstrated. We recently developed a temperature monitoring system based on the TDMA scheme, and demonstrated the parallel interrogation of 4 sensors shown in Fig. 1. This system is compliant with the frequency regulations for short range devices operated in the ISM band at 2.45 GHz. In this paper, we report the latest status of our development and present the fundamental relationship between the SNR (signal to noise ratio) of reflector responses and achievable time delay or phase accuracy, which is essential for designing the sensor system.

This work was supported in part by the Shinsei Foundation.

II. SENSOR PRINCIPLE

The principle of the temperature sensor is based on the temperature dependence of the propagation velocity of the surface acoustic wave and the thermal expansion of the substrate. The typical layout of the SAW sensor and its simulated time response is shown in Fig. 2. A radio wave emitted from a transceiver is received by an antenna, and SAWs are generated by an interdigital transducer (IDT) connected to the antenna. The surface wave propagates along the piezoelectric substrate, reflects at reflectors, and then returns to the IDT. The returned SAW is reconverted to a radio wave, which is transmitted back to the transceiver. Any mechanical deformation of the substrate or change in the propagation velocity occurring between the IDT and the reflectors results in a change of the delay time of the returned signal. The basis of using SAW delay line sensors is to relate variations in the reflector delay times to a measurand.

In this study black 128°YX $LiNbO_3$ was used as the piezoelectric substrate material. $LiNbO_3$ is often used for SAW devices as it features large piezoelectric coupling, which is important for low-loss and wide-band SAW transducers, negligible excitation of bulk waves, and a moderate temperature dependence of the SAW velocity. The chemical reduction of $LiNbO_3$ is effective to reduce pyroelectric effects, causing charge-up problems during fabrication and operation. As shown later, direct electron beam exposure of black $LiNbO_3$ substrates without the use of a conductive coating was used for the fabrication of the SAW sensors developed in this study.

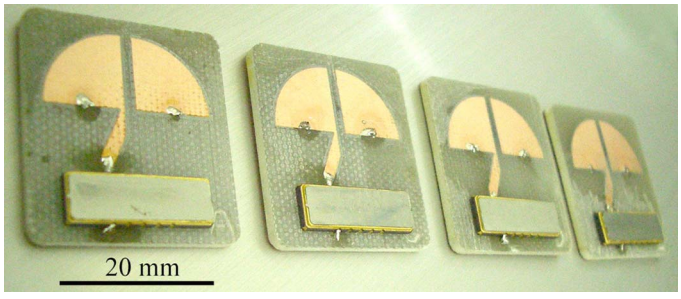

Figure 1. Developed 2.45 GHz wireless temperature transponders, consisting of packaged SAW delay line sensors mounted on a microstrip antenna.

A. *Temperature Sensitivity*

The temperature coefficient of delay (TCD), which is the rate of change in time delay of a SAW caused by a temperature variation, is defined as

$$\mathrm{TCD} = \frac{1}{\tau}\frac{\partial \tau}{\partial T} = \frac{1}{l}\frac{\partial l}{\partial T} - \frac{1}{v_0}\frac{\partial v_0}{\partial T} = \alpha - \frac{1}{v_0}\frac{\partial v_0}{\partial T}. \quad (1)$$

The first term in (1) corresponds to the thermal expansion coefficient of the substrate along the SAW propagation direction, which is found as 15.4 ppm/K [4]. The latter term corresponds to the change in the SAW velocity which is computed as -55.8 ppm/K based on a temperature-dependent implementation of the method given by [5] using material data from [4][6]. The resulting TCD for 128°YX $LiNbO_3$ is 71.2 ppm/K.

B. *Time Delay Dependence*

The temperature dependent formulation of a time delay τ is represented by

$$\tau(\Delta T) = \tau_0(1 + \mathrm{TCD} \cdot \Delta T), \quad (2)$$

where τ_0 refers to the initial time delay, and ΔT to the temperature variation. The sensitivity for a given time delay is thus

$$S_\tau = \frac{\partial \tau}{\partial T} = \tau_0 \mathrm{TCD}, \quad (3)$$

suggesting that the temperature sensitivity for a typical time delay of $\tau_0 = 1$ µs is approximately 0.07 ns/K. Increasing the sensitivity requires either a material with larger TCD or larger time delay. For 128°YX $LiNbO_3$ 1 µs of time delay corresponds to a chip length of ca. 2 mm. Larger time delays are obtained using a longer chip, however the propagation loss at 2.45 GHz increases at 5~6 dB/µs.

C. *Phase Dependence*

Higher sensitivity is achieved by evaluating the phase of the complex time response for a given reflector delay. The phase is related to the time delay as $\varphi = 2\pi f\tau$, where the frequency f corresponds to the center frequency of 2446 MHz. From (3) the temperature sensitivity of the phase is represented as

$$S_\varphi = \frac{\partial \varphi}{\partial T} = 2\pi f \tau_0 \mathrm{TCD}. \quad (4)$$

The temperature sensitivity for a typical time delay of $\tau_0 = 1$ µs is 63°/K, suggesting that high sensitivity is achieved even by a low-accuracy phase measurement. However, one phase value corresponds to many temperatures at intervals of 5.7 K (= 360°/63°/K), and a unique temperature cannot be determined just by evaluating the phase. Hereafter, this is referred to as "phase ambiguity".

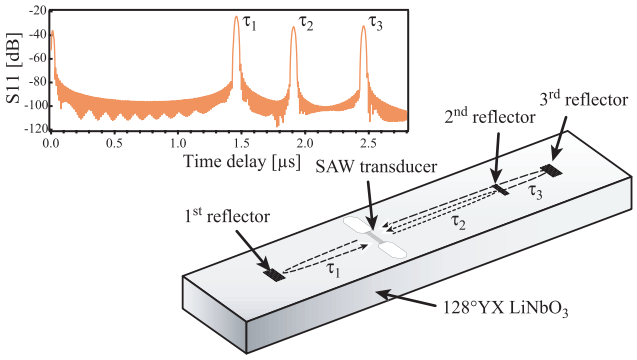

Figure 2. Typical structure of a one port SAW delay line sensor.

III. Multi-Step Evaluation Scheme

A multi-step evaluation scheme, which uses both time delay and phase, is adopted to achieve both high accuracy and wide range in temperature measurement. The multi-step evaluation scheme is illustrated in Fig. 3. At first, the largest and thus most sensitive relative time delay (e.g. $\tau_{31} = \tau_3 - \tau_1$ in Fig. 2) is chosen for the first rough temperature estimation. Because the time delay and phase depend on the distance of the free space propagation between the sensor and interrogation unit, antenna phase, the length of cables etc., only relative time delays and phases are employed. The temperature accuracy for this first evaluation is low judging from the achievable resolution of time delay measurement and the sensitivity determined by (2). Therefore, the following resolution refinement is performed using a relative phase. At this time, the temperature range corresponding to a phase change of 2π ($= 360°/S_\varphi$) must be smaller than the uncertainty of temperature determined using the time delay to avoid the phase ambiguity problem. Otherwise, one phase might correspond to two or more temperatures in an uncertainty of the first temperature evaluation. Therefore, a sufficiently small time delay is required for this second temperature evaluation (see (2)(4)). The required

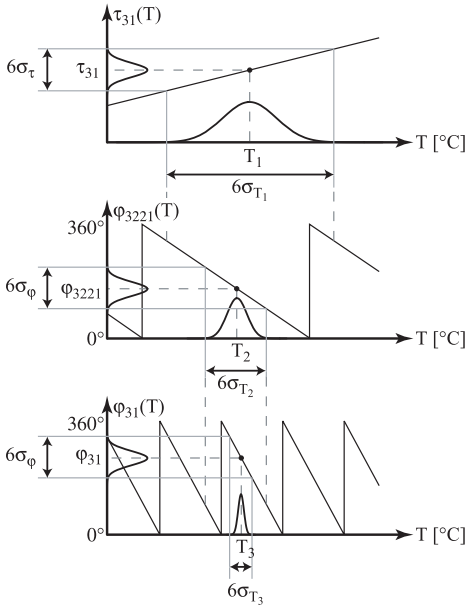

Figure 3. Principle of the three-step combined delay and phase evaluation scheme for temperature measurement.

time delay is thus created as a delay difference using three reflectors, as

$$\tau_{3221} = \tau_{32} - \tau_{21} = (\tau_3 - \tau_2) - (\tau_2 - \tau_1). \quad (5)$$

Evaluating the phase φ_{3221} of this delay results in an increased accuracy of the sought-after temperature. Further resolution refinement is performed using a more sensitive phase, which corresponds to a longer time delay. Again, the temperature range corresponding to a phase of 2π must be smaller than the uncertainty of the temperature determined using φ_{3221}. In our design, the most sensitive phase φ_{31}, can be used for this second resolution refinement.

IV. SNR Dependence of the Accuracy

The implementation of the proposed multi-step evaluation scheme requires the knowledge of the achievable accuracy for a time delay or phase measurement. However, this achievable accuracy depends on the positioning of the sensors and the transceiver antenna, obstructions, transceiver power, antenna gain, environmental noise etc. All of these factors can be related to the SNR of the sensors, and thus we must know the relationship between the SNR of the reflector responses and the achievable accuracy of the time delay or phase.

A. Experimental Evaluation

The achievable time and phase accuracy was experimentally evaluated using a 2.45 GHz frequency modulated continuous wave (FMCW) unit (Siemens SOFIS Module) with a bandwidth of 75 MHz, a center frequency of 2446 MHz, a sweep time of 1 ms, a transmitting power of +2 dBm and 1024 sampling points. The system uses a FMCW radar principle [7]. The time domain data is retrieved by applying windowing, zero-padding, and performing FFT. The exact delay time is found by fitting a spline function to three points closest to the peaks [3]. For the phase evaluation the real and imaginary part of the return loss are separately interpolated by spline functions, evaluated at the previously determined delay time, and normalized. In this experiment, the SNR was controlled by varying the orientation of the transceiver antenna during the wireless interrogation of the fabricated sensors. The SNR of each reflector response is defined as the ratio of its return loss and the background noise level, and hereafter will be referred to as SNR_i corresponding to the SNR of reflector *i*.

B. Accuracy of Absolute Time Delay

The sought-after relationship of the time delay accuracy versus the reflector SNR could be obtained by graphing the accuracy of e.g. τ_1, $\sigma(\tau_1)$ versus SNR_1. However, the accuracies of the absolute reflector time delays (τ_1, τ_2 and τ_3) versus their corresponding SNRs do not show a consistent relationship in this experiment. Further examination reveals that the error of each absolute time delay is not independent. As seen later, the relative time delays do follow a conclusive trend unlike the absolute time delays. These results suggest that some effects in the reader unit cause a random offset in the time delay and thus simultaneously affect all absolute time delays, but cancel for relative time delays such as τ_{31}.

C. Accuracy of Relative Time Delay and Phase

Logarithmically plotting the accuracies of the relative time delays τ_{31}, τ_{32}, τ_{21} and τ_{3221} versus SNR_1, nicely shows linear relationships. Although these lines are parallel, there is a slight offset between the accuracies of different relative delays. This suggests that there is a general relationship between the time delay accuracy σ_τ and SNR as

$$\sigma_\tau(\mathrm{SNR}) = exp(-c_1 \cdot \mathrm{SNR} - c_0), \quad (6)$$

where SNR has the units dB. It is obvious that a relative time delay using two reflectors depends on both the reflector SNRs. For example, $\sigma_{\tau_{31}}$ is a function of SNR_3 and SNR_1, $\sigma_{\tau_{31}}(SNR_3, SNR_1)$. However, we can introduce an effective SNR, which is a function of both reflector SNRs, e.g. $SNR_{31}(SNR_3, SNR_1)$. Using this effective SNR, the accuracy of the relative time delay τ_{31} can be represented as

$$\sigma_{\tau_{31}}(\mathrm{SNR}_3, \mathrm{SNR}_1) = \sigma_{\tau_{31}}(\mathrm{SNR}_{31}) = exp(-c_1 \cdot \mathrm{SNR}_{31} - c_0), \quad (7)$$

based on the discussion for (6). What we want to do below is to determine c_0 and c_1 using the experimental results.

D. Definition of the Effective SNR

The accuracy of the relative time delay τ_{31}, $\sigma_{\tau_{31}}$, can be related to the accuracy of τ_3 and τ_1 as

$$\sigma_{\tau_{31}}(\mathrm{SNR}_{31}) = \sqrt{\sigma_{\tau_3}(\mathrm{SNR}_3)^2 + \sigma_{\tau_1}(\mathrm{SNR}_1)^2} \quad (8)$$

assuming that the τ_3 and τ_1 are independent. After substituting (7) into (8) and replacing the accuracies of σ_{τ_3} and σ_{τ_1} with the general assumed relation of (6), we can solve the resulting equation for SNR_{31}, obtaining

$$\mathrm{SNR}_{31} = -\frac{c_0}{c_1} - \frac{1}{2c_1} ln(e^{-2c_0}[e^{-2c_1\mathrm{SNR}_3} + e^{-2c_1\mathrm{SNR}_1}]). \quad (9)$$

The coefficients c_0 and c_1 are obtained by fitting (6) to the measured relationship of the time delay accuracy versus the effective SNR. This recursive problem is solved by iterating this fitting procedure, converging after 4 cycles. Instead of repeating this procedure for each relative time delay, the effective SNR is derived simultaneously for all relative delays based on one best

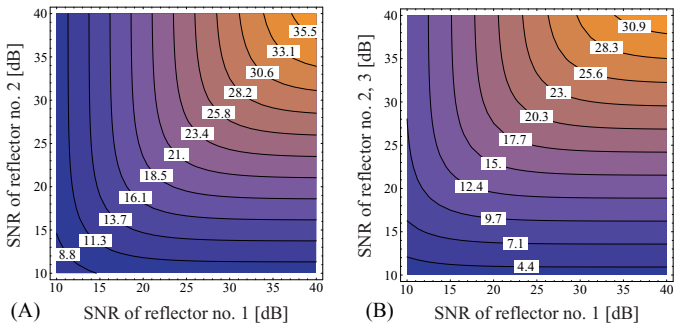

Figure 4. Relation of the reflectors SNRs to the effective SNR used in Fig. 5 for a relative time delay or phase using 2 reflectors (A) and 3 reflectors (B), assuming that the SNR of reflectors two and three are identical.

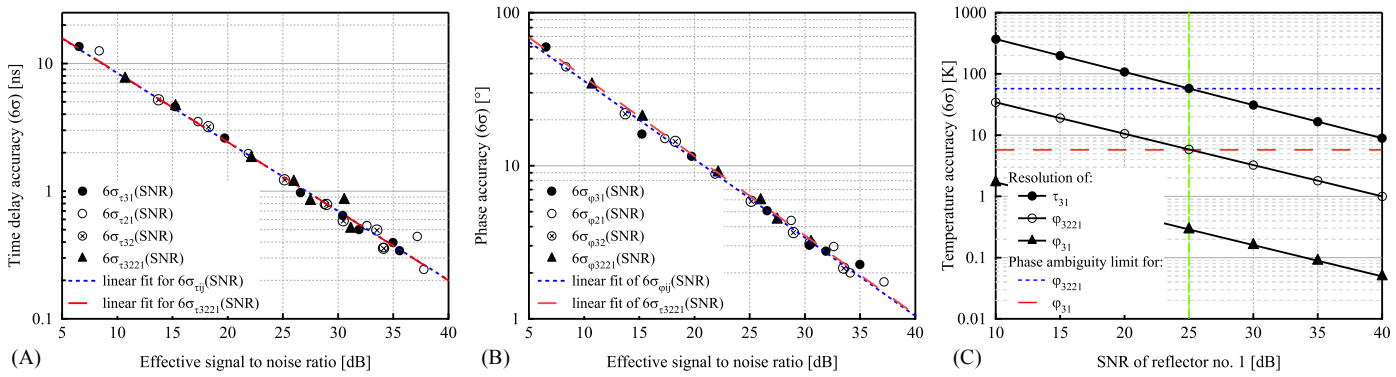

Figure 5. Experimentally derived relation of the achievable time delay (A) and phase accuracy (B) for an effective SNR. The expected temperature accuracy for the fabricated TDMA based sensors is shown in (C).

fit of all data. The resulting relation of the effective SNR is illustrated in Fig. 4 (A), which is used for plotting the achievable time delay and phase accuracies shown in Fig. 5 (A) and (B), respectively.

The approach to derive the effective SNR for a relative time delay involving three reflectors, as for τ_{3221}, is identical, except that the repeated occurrence of τ_2 in (5) must be taken into account [8]. This leads to a slightly modified expression of (8) as

$$\sigma_\tau(\mathrm{SNR}_{3221}) = \sqrt{\sigma_\tau(\mathrm{SNR}_3)^2 + (2\sigma_\tau(\mathrm{SNR}_2))^2 + \sigma_\tau(\mathrm{SNR}_1)^2}. \quad (10)$$

This procedure also converges after 4 iterations. The derived expression relating the three reflector SNRs to the effective SNR is shown in Fig. 4 (B), where it has been assumed that SNR_2 and SNR_3 are identical, which is true for the developed sensors. As seen from Fig. 5 (A) and (B), the experimental data using this definition of the effective SNR for three reflectors agrees well with the delay accuracy based on using two reflectors. The conclusive agreement of the accuracies for both relative time delay and phase support this procedure and the choice of the ansatz function (6).

E. SNR based Design of Reflector Time delays

Fig. 5 (C) shows the temperature accuracy related to the SNR of the first reflector for the fabricated TDMA sensors with the properties of the sensors given in Table I. Hereby, the SNR of reflectors 2 and 3 were related to the SNR of reflector 1 based on the simulated return loss of Table I, that is e.g. $\mathrm{SNR}_3 = \mathrm{SNR}_1 - 8.1$ dB. Based on (4), the phase ambiguities are computed for φ_{3221} and φ_{31}, and it is found that phase ambiguity occurs if the temperature range exceeds 57.4 K and 5.74 K, respectively. Fig. 5 (C) confirms that an SNR_1 larger than 25 dB in the measurement of τ_{31} is sufficient to prevent the phase ambiguity of φ_{3221}. Similarly, the temperature accuracy for φ_{3221} at 25 dB is high enough to avoid the phase ambiguity of φ_{31}. The accuracy improvement effect by the three-step evaluation scheme is estimated using Fig. 5 (C). The improvement of factor 10 is achieved by switching from τ_{31} to φ_{3221}, and the further improvement of factor 20 is achieved by switching from φ_{3221} to φ_{31}. In total, this leads to an overall accuracy increase of factor 180~220, depending on the SNRs.

V. Sensor Design

The SAW simulation of the delay line sensors was performed based on the K-Model [9], including all significant higher order effects. The aluminum metallisation thickness of 50 nm ($h/\lambda = 3.2$ %) was selected to compensate the internal reflections in the IDT, as suggested in [9]. The electrode width at the center frequency of 2442 MHz for electrically shorted and open electrodes was determined to be 395 nm and 401 nm, respectively, based on data from [10]. The acoustic track width of 80 λ_0 was determined by comparing the losses originating from the electrode resistance and SAW diffraction for an average time delay. The IDT was then designed to match the input resistance to 50 Ω using one serial matching inductor, assuming a sheet resistance of $R_\square = 1.9$ Ω/□. It is found from the simulation that the input resistance of 50 Ω is achieved for an IDT with 27 electrodes, corresponding to a bandwidth of 161 MHz (VSWR < 2).

The reflector structures were chosen to be electrically open, as the reflectivity due to mass loading and electrical loading add constructively on 128°YX $LiNbO_3$. As reflectors 2 and 3 are placed in the same acoustic track, the design objective was to obtain identical return loss for both τ_2 and τ_3. Based on the reflector return loss and exact time delay extracted from the simulation the number of reflector electrodes and the exact

TABLE I. Simulated and Measured Properties[a] of the 2.45 GHz SAW Delay Line Temperature Sensors

Sensor ID	R_{in} [Ω]	C_0 [pF]	L_s [nH]	τ_1 [µs]	α_1 [dB]	τ_2 [µs]	α_2 [dB]	τ_3 [µs]	α_3 [dB]
Simulation (K-Model)									
A	51.7	0.59	2.4	1.460	-24.0	1.910	-32.8	2.460	-32.1
B	51.7	0.59	2.4	1.570	-24.6	2.020	-33.4	2.570	-32.7
C	51.7	0.59	2.4	1.680	-25.3	2.130	-34.1	2.680	-33.4
D	51.7	0.59	2.4	1.790	-25.9	2.240	-34.7	2.790	-34.0
Measurement									
A	51.6	0.62	2.8	1.462	-25.2	1.913	-31.6	2.464	-33.6
B	51.8	0.62	2.8	1.572	-26.1	2.024	-32.0	2.574	-34.2
C	52.2	0.61	2.8	1.682	-27.0	2.134	-32.5	2.684	-34.7
D	54.7	0.58	2.8	1.792	-27.7	2.244	-33.4	2.794	-35.7

a. R_{in} refers to the input resistance of the sensor, C_0 to the static capacitance, L_s to the calculated serial matching inductance, τ_i and α_i to the to the delay time and return loss of reflector i, respectively.

reflector position on the chip were determined. The number of the reflector electrodes were chosen to be 61 for τ_1 and τ_3, and 11 for τ_2.

VI. Fabrication

The SAW delay line senors were fabricated on chemically reduced (black) 128°YX $LiNbO_3$ using direct writing with a electron beam lithography (EBL) system (JEOL JBX-5000LS). The electrode pattern was formed by patterning 400 nm thick ZEON ZEP520A positive type electron beam (EB) resist with a dose of 88 μC/cm^2 at a beam current of 100 pA and 50 kV acceleration voltage. Subsequently, 5 nm thick titanium (Ti) and 50 nm thick aluminium (Al) were deposited by electron beam evaporation. The Ti layer improves the adhesion and temperature stability of the Al metallisation [11]. The bond pad and bus bars were formed by another lift-off step using image reversal resist (Clariant AZ5214E) and evaporating 50 nm thick Ti and 700 nm thick Al.

The direct EB exposure of black $LiNbO_3$ substrates was performed without use of an anti-charge-up coating. Generally, the EB exposure of piezoelectric substrates requires the coating of a thin conductive layer in order to prevent charge up effects. However, we found that the conductivity of chemically reduced $LiNbO_3$ is sufficient to prevent these effects even for a dose as high as 130 μC/cm^2. Although only a small section of the bus bar is written during the EBL, proximity effects lead to a distortion of the designed electrode structures, as seen in Fig. 6 (A). Proximity effects lead to a broadening of the electrode towards the bus bars and narrowing of the electrode at the outside of the IDT. In order to determine the proximity parameters experimentally, we patterned arrays of metal lines with constant width, but varying pitch. After the lift-off of a thin metal layer, the electrode line widths were measured in a scanning electron microscope. The measured distribution of the electrode widths were then compared to simulated ones for varying pitches. The line width simulation was based on the proximity function given as [12]

$$f(r) = \frac{1}{(1+\eta)\pi}\left[\frac{1}{\alpha^2}exp\left(-\frac{r^2}{\alpha^2}\right) + \frac{\eta}{\beta^2}exp\left(-\frac{r^2}{\beta^2}\right)\right], \qquad (11)$$

where r, α, β and η represent the distance from the beam center, the forward scattering coefficient, the back scattering coefficient and the ratio of total energy deposited by the back scattered electrons compared to the forward scattered electrons, respectively. The best fit parameter set was $\alpha = 0.212$ μm, $\beta = 4.6$ μm, and $\eta = 0.34$. Based on this dose distribution, the exposed pattern of the IDT and reflectors were modified to yield the designed shape. Fig. 6 (B) shows the improved result for the corrected IDT structure.

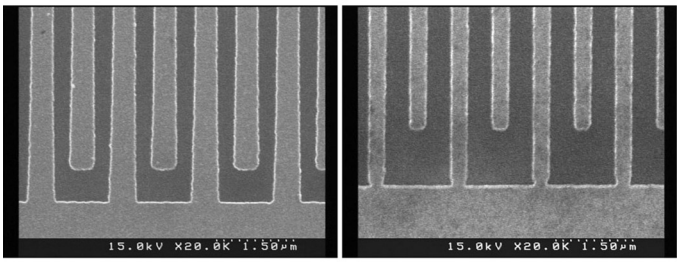

(A) (B)

Figure 6. Structures of the fabricated interdigital transducer by direct electron beam lithography on chemically reduced 128°YX $LiNbO_3$ showing proximity effects (A), and the results using EB dose simulation and corrected CAD (B).

VII. Results

A. Evaluation of Time Delay Sensors

The fabricated sensors were characterized using a Agilent ENA5071B network analyzer and a CASCADE ACP40 GS probe. The extracted sensor values are given in Table I, showing close agreement with the K-Model simulation. The delay times are estimated accurately within 4 ns (< 0.2 %), and the return loss within 1.8 dB. The requirements for the designed 50 Ω input resistance and serial inductance matching were also closely met. A comparison of the simulated and measured time response is shown in Fig. 7.

B. Temperature Evaluation

Diced sensors were mounted in ceramic SMD SAW packages using high temperature epoxy and wire bonded. The packaged sensors were attached to micro strip antennas fabricated using 2.0 mm thick FR4. As antenna a wide band patch antenna, referred to as "Compact gap-coupled shorted 90° sectoral microstrip antenna" [13] was used. This antenna was designed to have a front-side strip line feed, including a matching section as to achieve the intended matching including the bondwire inductance.

The four parallel sensors were interrogated using a Siemens SOFIS Module and a circular polarized antenna having a gain of 14.5 dBi. The temperature characteristics were evaluated by placing the four sensors in an oven with a glass window, which was positioned about 30 cm from the reader antenna. A Pt100 sensor was used as a temperature reference. In order to minimize temperature differences between the sensors under test and the reference, the data was acquired during the cool-down of the oven, preventing temperature fluctuations resulting from the on/off control of the heater.

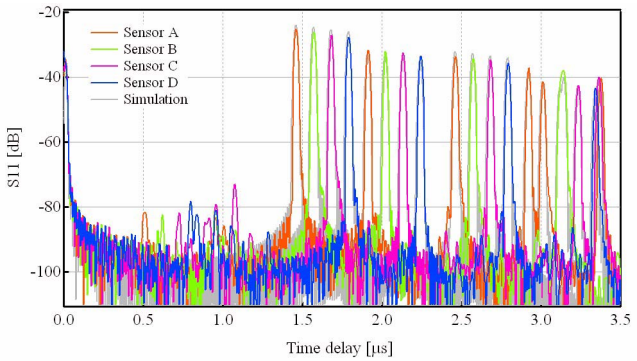

Figure 7. Time domain response of fabricated SAW delay line sensors (A-D) showing close agreement with the K-model simulation (gray lines).

The extracted delay and phase data of τ_{31}, φ_{3221} and φ_{31} for the sensor D are shown in Fig. 8. Computed TCDs for each relative time delay TCD_{31}, TCD_{32}, TCD_{21}, and TCD_{3221} are 64.3, 87.2, 36.4, and 319.8 ppm/K, respectively. However, they, especially TCD_{21} and TCD_{3221}, are considerably different from the theoretical value of 71.2 ppm/K. This could be ascribed to a non-uniform TCD originating from mounting the chip with high temperature epoxy and the difference in expansion coefficients of the sensor chips and the package, and is discussed in detail in [14]. The TCD extracted from the phase evaluation for φ_{3221} and φ_{31} based on (4) is 127.2 ppm/K and 57.5 ppm/K, yielding phase ambiguity intervals of 32.1 K and 7.1 K, respectively. Due to the reduced ambiguity interval of φ_{3221} a SNR larger than 30.5 dB is required for reflector 1 to prevent phase ambiguity. The temperature accuracy at 30.5 dB and 35.5 dB is 0.19 K and 0.1 K (6σ), corresponding to a read-out distance of 140 cm and 130 cm, respectively.

The issue of differing TCD was solved for a new sensor series fixing the sensor chips solely at the edge, and thus outside of the acoustic track. For this case, the results agree well with the assumption of a uniform TCD, and phase ambiguity is prevented for an SNR larger than 25 dB, as designed.

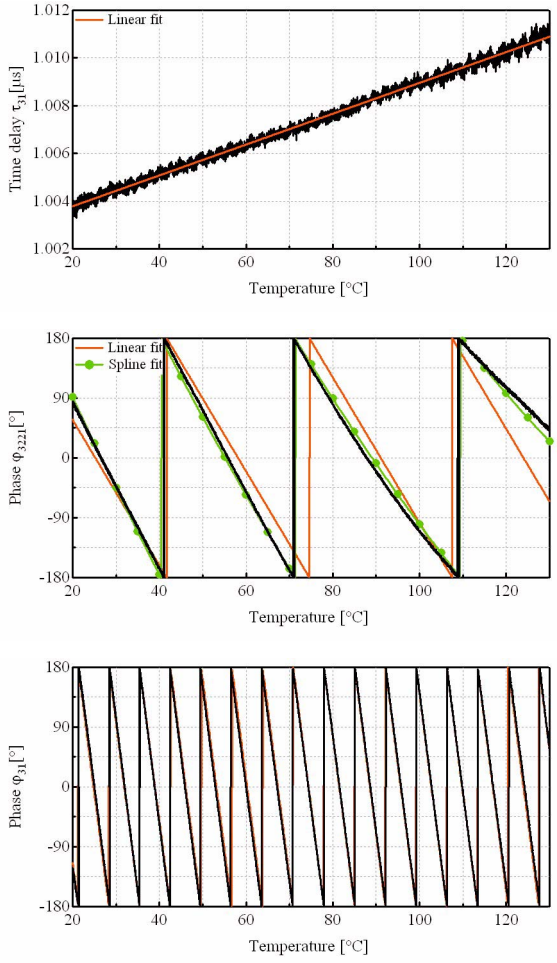

Figure 8. Measured temperature characteristics of the delay and phase differences for the three-step evaluation scheme.

VIII. CONCLUSION

A wireless temperature sensor system operating in the 2.45 GHz ISM band featuring parallel sensor interrogation was demonstrated. A multi-step evaluation scheme based on time delay and phase evaluation is proposed, leading to an accuracy improvement of factor 200 compared to a simple time delay evaluation. A fundamental relationship of time delay and phase accuracy for an effective SNR is introduced, which allows for an exact design of the proposed evaluation scheme and prevents phase ambiguities. Close agreement between the SAW simulation and fabricated sensors was achieved, with an accuracy below 4 ns for the time delay and 1.8 dB for the return loss. In this first demonstration of TDMA (time division multiple access) sensors, the temperature accuracy of 0.19 K (6σ) was achieved at a transmission power of +2 dBm (1.59 mW), when the distance between the transceiver and sensors was about 1.4 m.

ACKNOWLEDGMENT

J. H. K. would like to thank C. Seisenberger with the SIEMENS AG for the continuous support concerning the Siemens SOFIS Module used in this study.

REFERENCES

[1] X. Q. Bao, W. Burghard, V. V. Varadan, and K. V. Varadan, "SAW Temperature Sensor and Remote Reading System", Proc. IEEE Ultrason. Symp.1987, pp. 583-585

[2] L. Reindl, G. Scholl, T. Ostertag, H. Scherr, U. Wolff, F. Schmidt, "Theory and application of passive SAW transponders as sensors", IEEE Trans. Ultra. Ferro. Freq. Cont., vol. 45, no. 5, 1998, pp. 1281-1292

[3] L. M. Reindl, I. M. Shrena, "Wireless measurement of temperature using surface acoustic waves sensors", IEEE Trans. Ultra. Ferro. Freq. Cont., vol. 51, no. 11, 2004, pp. 1457-1463

[4] R. T. Smith, and F. S. Welsh, "Temperature dependence of the elastic, piezoelectric, and dielectric constants of Lithium Tantalate and Lithium Niobate", J. Appl. Phys., vol. 42, no.6, 1971, pp. 2219-2230

[5] J. J. Campbell, W. R. Jones, "A method for estimating optimal crystal cuts and propagation directions for surface waves", IEEE Trans. Sonics Ultrason., vol. SU-15, no. 4, 1968, pp. 209-217

[6] G. Kovacs, M. Anhorn, H. E. Engan, G. Visintini, and C. C. W. Ruppel, "Improved material constants for $LiNbO_3$ and $LiTaO_3$", Proc. IEEE Ultrasonics Symp. 1990, pp. 435-438

[7] M. I. Skolnik, "Introduction to radar systems", 3rd ed., Mc Graw Hill, pp. 193-197

[8] J. R. Taylor, "An introduction to error analysis", 2nd ed., University Science Books, pp. 143-144

[9] J. H. Kuypers, D. A. Eisele, L. M. Reindl, "The K-Model - Green's Function based analysis of surface acoustic wave devices", Proc. IEEE Ultrasonics Symp. 2005, pp. 1550-1555

[10] K. Ibata, T. Omori, K. Hashimoto, M. Yamaguchi, "Polynomial expressions for SAW reflection by aluminium gratings on 128°YX-$LiNbO_3$", Proc. IEEE Ultrason.Symp.1998, pp. 193-197

[11] C. A. Johnsen, J. L. Henderson, "Improved metallization for SAW filters on $LiNbO_3$", Proc. IEEE Ultrason.Symp.1986, pp. 97-101

[12] A. Misaka, K. Harafuji, N. Nomura, "Determination of proximity effect parameters in electron-beam lithography", J. Appl. Phys. 68, 1990, pp. 6472-6479

[13] K. P. Ray, G. Kumar, "Compact gap-coupled shorted 90° sectoral microstrip antenna", Microw. a. Opt. Tech. Lett., vol. 26, No. 3, 2000

[14] J. H. Kuypers, D. A. Eisele, L. M. Reindl, S. Tanaka, M. Esashi, "2.45 GHz passive wireless temperature monitoring system featuring parallel sensor interrogation and resolution evaluation", Proc. IEEE Sensors 2006, in press